Journal of Engineering Science and Technology
Vol. 12, No. 5 (2017) 1366 - 1385

MVDR ALGORITHM BASED LINEAR ANTENNA ARRAY PERFORMANCE ASSESSMENT FOR ADAPTIVE BEAMFORMING APPLICATION

SUHAIL NAJM SHAHAB[1,2,*], AYIB ROSDI ZAINUN[1], HUSSIEN AHMED ALI[3], MOJGAN HOJABRI[1], NURUL HAZLINA NOORDIN[1]

[1]Faculty of Electrical and Electronics Engineering, Universiti Malaysia Pahang, 26600, Pahang, Malaysia
[2]Department of Electrical techniques, Al-Hawija Technical Institute, Northern Technical University, Iraq
[3]College of Science, Computer Science Department, Kirkuk University, Iraq
*Corresponding Author: 68suhel@gmail.com

Abstract

The performance of Minimum Variance Distortionless Response (MVDR) beamformer is sensitive to errors such as the steering vector errors, the finite snapshots, and unsatisfactory null-forming level. In this paper, a combination of MVDR with linear antenna arrays (LAAs) for two scanning angles process in the azimuth and elevation are used to illustrate the MVDR performance against error which results in acquiring the desired signal and suppressing the interference and noise. The impact of various parameters, such as the number of elements in the array, space separation between array elements, the number of interference sources, noise power level, and the number of snapshots on the MVDR are investigated. The MVDR performance is evaluated with two important metrics: beampattern of two scanning angles and Signal to Interference plus Noise Ratio (SINR). The results found that the MVDR performance improves as the number of array elements increases. The beampattern relies on the number of elements and the separation between array elements. The best interelement spacing obtained is 0.5λ that avoids grating lobes and mutual coupling effects. Besides, the SINR strongly depends on the noise power label and a number of snapshots. When the noise power label increased, the MVDR performance degraded as well the null width increases in the elevation direction as well as more accurate resolution occurred when the number of snapshots increased. Finally, it is found the proposed method achieves SINR better than existing techniques.

Keywords: Beamforming algorithm, Linear antenna array, Minimum variance distortionless response, MVDR, SINR, Smart antenna.

Nomenclatures

$a(\theta_i, \phi_i)$	Steering vector for the interference source
$a(\theta_s, \phi_s)$	Steering vector for the desired signal
d	Interelement spacing
$E[.]$	Expectation operator
Id_L	L×L identity matrix
j	Imaginary unit
L	Number of elements
ns	Snapshots
$P(\theta, \phi)$	Mean output power
q	Wave number
R_{i+n}	Interference plus noise covariance matrix
R_s	SOI covariance matrix
R_y	Theoretical covariance matrix
w	Complex weight vector
$y(t)$	Array output
$(.)^H$	Conjugate transpose (Hermitian transpose)
$(.)^T$	Transpose operator
$x_i(t)$	Interference signal
$x_n(t)$	White Gaussian noise
$x_s(t)$	Desired signal
$x_T(t)$	Total received signal

Greek Symbols

$\nabla\xi(t)$	Gradient vector
θ	Azimuth angle
λ	Signal wavelength
ϕ	Elevation angle
μ	Step size parameter
σ_i^2	Interference power
σ_n^2	Noise power
σ_s^2	Power of the desired signal

Abbreviations

ABF	Adaptive Beamforming
AoA	Angle of Arrival
BF	Beamforming
BS	Base Station
CGM	Conjugate Gradient Method
DBF	Digital Beamforming
DoA	Direction of Arrival
LAA	Linear Antenna Array
LMS	Least Mean Square
LTE	Long Term Evolution
MDN	Maximum Depth Null
MLBw	Main Lobe Beamwidth
MSLL	Maximum Side Lobe Level

MVDR	Minimum Variance Distortionless Response
RAA	Rectangular antenna array
RLS	Recursive Least Square
SINR	Signal to Interference plus Noise Ratio
SNR	Signal to Noise Ratio
SMI	Sample Matrix Inversion
SNOI	Signal Not of Interest
SOI	Signal of Interest

1. Introduction

Currently, the mobile cellular networks are experiencing a massive evolution of data traffic, because of multimedia and internet applications that are used by a vast number of devices such as smartphones, mobile PC, and tablets [1, 2]. Most beamforming techniques have been considered for use at the base station (BS) since antenna arrays are not feasible at mobile terminals due to space limitations [3].

With the increasing trend of the number of subscribers and demand for different services in wireless systems, there are always requirements for better coverage, higher data rate, improved spectrum efficiency and reduced operating cost. To fulfill this requirement, beamforming technique is able to focus the antenna array pattern into a particular direction and thereby enhances the desired signal power. Interference is one of the significant obstacles in the wireless networks. It can be caused by other users or by the signal itself [4]. The signal can interfere with itself due to multipath components, where the signal is gathered with another version of the signal that is delayed because of another propagation path [5]. The fundamental principle of the Adaptive beamforming (ABF) algorithm is to track the statistics of the surrounding interference and noise field as well as adaptively seek for the optimum nulls location that decreases the interference and noise dramatically under the restriction that the desired signal is not distorted at the beamformer's output [6]. The basic idea of the Minimum Variance Distortionless Response (MVDR) algorithm or Capon beamformer [7] is to estimate the beamforming coefficients in an adaptive way by minimizing the variance of the residual noise and interference while enforcing a set of linear constraints to ensure that the desired signals are not distorted [6].

Lin et al. [8] proposed an enhanced model of MVDR algorithm by changing the position of the reference element in steering vector to be in the middle of the array and the number of elements must be odd. Simulation results show that modified MVDR has a realistic behavior especially for detecting the incoming signals direction and outperforms the conventional MVDR. One of the popular approaches to improving the classic Capon beamformer in the presence of finite sample effect and steering vector errors is the diagonal loading, which was studied by Manolakis et al. [9]. The idea behind diagonal loading is to adapt a covariance matrix by adding a displacement value to the diagonal elements of the estimated covariance matrix. Nevertheless, how to select an appropriate diagonal loading level is a challenging task. Das and Sarma [10] mentioned that the element spacing must be $\lambda/2$ to prevent spatial aliasing. Choi et al. [11] presented a comparative study of MVDR algorithm and LMS algorithm, where results show that LMS is the better performer. The SINR maximization is another criterion employed in the joint transmitter and receiver beamforming algorithms [12-14]. Ku et al. [15] analysed the mixing of a differential algorithm based linear antenna

array is applied to deepen nulls and lower side lobe levels (SLLs) in the unwanted direction, and they found the max null depth of -63dB by using 20-elements. The statistic numerical algorithm was proposed to obtain the requirement for the amplitude and phase error of multi-beam active phased array antenna [16].

The radiation beampattern is simulated from the value of the random amplitude and phase errors of the phase shifter. From the results, it is found that the only way to meet the requirement of the SLL is to use digital beamforming (DBF). The researchers in [7] investigate the performance of the MVDR beamformer for four different types of noise and source incidence angles using Signal to Noise Ratio (SNR) and beampattern as the evaluation criteria. An evaluation of the trade-off between noise reduction and reverberation of the MVDR filter is presented in [17]. Mu et al. [18] compared the performance of four different BF methods which is the Least Mean Square (LMS), Sample Matrix Inversion (SMI), Recursive Least Square (RLS), and Conjugate Gradient Method (CGM). The comparison is based on the null-forming level, beamwidth, and the maximum SLL by varying the number of array elements and the separation between array elements. It found that the CGM is the best method that gives deep null with a minimum number of iterations. Another study of Shahab et al. [19] on MVDR algorithm based on reconstructing the covariance matrix for the SOI under the mismatch conditions. Recently, work on MVDR performance based on Rectangular Antenna Array (RAA) has been carried out by Lee [20], however, the MVDR performance show capability to combine with RAA but its need large number of antenna elements.

Smart antennas system (SAS) include signal processing capabilities that perform tasks such as the Direction of Arrival (DoA) estimation and beamforming. A smart antenna that is held in the BS of a cellular network consists of antenna arrays where the amplitudes are accustomed by a group of weight vectors using an ABF algorithm. Before ABF, the DoA estimation is used to specify the main directions of users and interferers. Previous research has analyzed the accuracy and precision of a proposed wideband capon beamforming for estimating the elevation angle, azimuth angle, and velocity for target parameters using planner antenna array [21]. The function of ABF algorithms is to form the main beam to the user direction and placing nulls towards interference and noise directions by adjusting the antenna itself using beamforming (BF) techniques to achieve better transmission or reception beam pattern which increases SINR by mitigating co-channel interference present in the wireless communication system. The ABF algorithm improves the output of the array beam pattern in a way which it maximizes the radiated power where it will be produced in the wanted users' direction. Moreover, deep nulls are placed in the unwanted signal directions that symbolize co-channel interference from desired users in the neighboring BSs.

So far, ABF is a function of the number of elements, spacing between adjacent elements, the angular separation between desired user and undesired signals, noise power level as well as a number of snapshots. Therefore, it is important to investigate the impact of these parameters on the beampattern in the azimuth and elevation scan angles that can introduce a sharp and deep null-forming towards the Signal-Not-of-Interest (SNOI) direction especially in the elevation angle while maximum power placed the majorlobe toward the Signal-of-Interest (SOI) direction. This paper includes simulation results and performance analysis of

MVDR algorithm, whereas no complete assessment of the SINR as a function of all the above-mentioned parameters. The analysis of the MVDR in this work is carried out in four different scenarios where the MVDR performance is assessed with two important metrics; beampattern for azimuth and elevation scan angles and SINR. This analysis not only helps to better understand the MVDR beamformer but also helps to better design array systems in practical application. The remainder of this paper is organized as follows. In section 2, MVDR beamformer based on linear antenna array configuration with the signal propagation model is described. The simulation results and performance analysis are provided in Section 3. Finally, in Section 4, the paper's conclusions and summary of MVDR performance are described.

2. System Model and MVDR Beamformer

In this section, the mathematical formulation of the design model for adaptive beamforming will be presented in detail. Consider a single cell with L element antenna arrays. Let there be S wanted signal sources and I interference sources spreading on same the frequency channel at the same time. The algorithm starts by creating a real life signal model. A number of plane waves are considered from K narrowband sources impinging from various angles (θ, ϕ). The impinging radio frequency signal reaches into an antenna array from the far-field region to the array geometry of linear antenna arrays (LAAs). A block diagram of the antenna array using DoA and BF process is shown in Fig. 1. As displayed in this figure, after the signals are received by antenna arrays consisting of the wanted user signal, the interference source, and the noise, the first part is to estimate the direction of the arrival of the S signal and I signals using a well-known algorithm developed by Capon [7], named MVDR spectrum estimator, to find the DoA angles of several sources. However, the MVDR estimator algorithm wants information of the number of sources. With the known direction of the source, then the second part is applied by using MVDR ABF technique that places a straight beam to S signal and placing nulls in the direction of I signals. Each signal is multiplied by adaptable complex weights and then summed to form the system output.

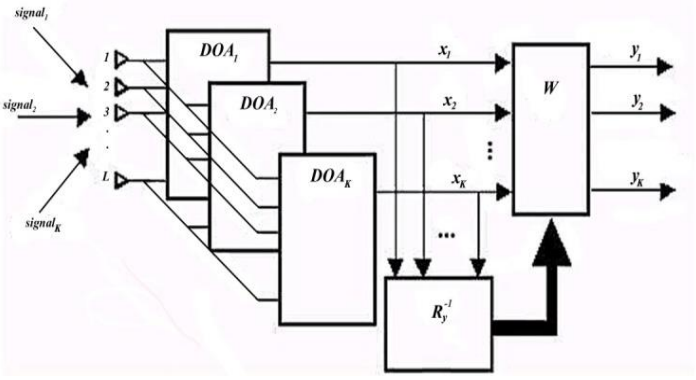

Fig. 1. A smart antenna array system using DoA and beamforming process.

The total composite signals received by an adaptive antenna array at time index, t, become:

$$x_T(t) = \sum_{s=1}^{S} x_s(t)\, a(\theta_s, \phi_s) + \sum_{i=1}^{I} x_i(t)\, a(\theta_i, \phi_i) + x_n(t) \tag{1}$$

where $x_T(t) \in C^{K \times L}$, $x_s(t)$, $x_i(t)$, $x_n(t)$, denote the desired signal, interference signal and noise added from White Gaussian noise, respectively. The unwanted signal consists of $x_i(t)+x_n(t)$ and I is the number of interferences, the desired angle and interference direction of arrival angles are θ_s and θ_i, i=1, 2…, I, respectively. $a(\theta_s,\phi_s)$ denote the steering vector or array response for wanted signal while $a(\theta_i, \phi_i)$ refers to the interference signal steering vector or array response to the unwanted signal. (θ, ϕ) composed of azimuth angle ∈ [0°, 2π°] and elevation angle ∈ [0°, π/2°]

Steering vector is a complex vector $\in C^{L \times K}$ containing the responses of all elements of the array to a narrowband source of unit power depending on the incident angle, which is given by [22]:

$$a(\theta,\phi) = [1, e^{-jqd\sin(\theta)\sin(\phi)}, e^{-jq2d\sin(\theta)\sin(\phi)}, \ldots, e^{-jq(L-1)d\sin(\theta)\sin(\phi)}] \tag{2}$$

where j is the imaginary unit, (i.e. $j^2 = -1$), d is the spacing between elements and q is the wave number given as:

$$q = 2\pi / \lambda \tag{3}$$

where λ refers to the received signal wavelength. The signal $x_T(t)$ received by multiple antenna elements is multiplied with a series of amplitude and phase (weight vector coefficients) which accordingly adjust the amplitude and phase of the incoming signal. This weighted signal is a linear combination of the data at L elements, resulting in the array output, $y(t)$ at any time t, of a narrowband beamformer, which is given by;

$$y(t) = \sum_{l=1}^{L} w^H x_T(t) \tag{4}$$

where $y(t)$ is the beamformer output, $x_T(t)$ is the antenna element's output, w is the complex weight vector for the antenna element = $[w_1, w_2, \ldots, w_L]^T$ is $\in C^{L \times 1}$ beamforming complex vector. $(.)^H$ and $(.)^T$ denotes the conjugate transpose (Hermitian transpose) of a vector or a matrix, which is used to simplify the mathematical notation and transposes operators respectively. The weight vector at time $t+1$ for any system that uses the immediate gradient vector $\nabla\xi(t)$ for weight vector upgrading and evades the matrix inverse operation, which is defined as follows:

$$w(t+1) = w(t) + \frac{1}{2}\mu[\nabla\xi(t)] \tag{5}$$

where μ is the step size parameter, the convergence speed control by μ and lies between 0 and 1. The smallest values of μ facilitate the high-quality estimation and sluggish concurrence, while huge values may result in a rapid union. However, the constancy over the minimum value may disappear. Consider

$$0 < \mu < 1/\lambda_{\max} \tag{6}$$

An instantaneous estimation of gradient vector is written as

$$\nabla\xi(t) = -2p(t) + 2R_y(t)\,w(t) \tag{7}$$

$$p(t) = d^*(t)x_T(t) \tag{8}$$

$$R_y = x_T(t){x_T}^H(t) \tag{9}$$

A precise calculation of $\nabla\xi(t)$ is not possible because prior information on cross-correlation vector, p and covariance matrix, R_y of the measurement vector are required. By substituting (8) with (6), the weight vector is derived as follows:

$$\begin{aligned} w(t+1) &= w(t) + \mu[\,p(t) - R_y(t)\,w(t)] \\ &= w(t) + \mu\,x_T(t)[d^*(t) - x_T(t)\,w(t)] \\ &= w(t) + \mu\,x_T e^*(t) \end{aligned} \tag{10}$$

The following three formulas can further define the desired signal:

$$y(t) = w^H(t)\,x_T(t) \tag{11}$$

$$e(t) = d^*(t).y(t)w(t+1) = w(t) + \mu\,x_T(t)e^*(t) \tag{12}$$

The covariance matrix, R_y is constructed conventionally with unlimited snapshots. However, it is estimated by using the limited snapshots signal in the actual application. It can be expressed as:

$$R_y = \sigma_s^2 a(\theta_s,\phi_s)a^H(\theta_s,\phi_s) + \sum_{i=1}^{I}\sigma_i^2 a(\theta_i,\phi_i)a^H(\theta_i,\phi_i) + \sigma_n^2 Id_L \tag{13}$$

$$R_s = \sigma_s^2 a(\theta_s,\phi_s)a^H(\theta_s,\phi_s) \tag{14}$$

$$R_{i+n} = \sum_{i=1}^{I}\sigma_i^2 a(\theta_i,\phi_i)a^H(\theta_i,\phi_i) + \sigma_n^2 Id_L \tag{15}$$

$$R_y = R_s + R_{i+n} = \mathrm{E}[x_T(t){x_T}^H(t)] \tag{16}$$

$$\sigma_s^2 = E[\left|x_s(t)\right|^2] \tag{17}$$

$$\sigma_i^2 = E[\left|x_i(t)\right|^2] \tag{18}$$

where R_y, σ_s^2 , σ_i^2 , σ_n^2 , Id_L, R_s, R_{i+n} and E[.] denotes, respectively, the $L\times L$ theoretical covariance matrix, power of the desired signal, interference power, noise power, $L\times L$ identity matrix, *SOI* covariance matrix, interference plus noise covariance matrix and expectation operator.

The common formulation of the MVDR beamformer that determines the $L\times 1$ optimum weight vector is the solution to the following constrained problem [23]:

$$w_{MVDR} = \arg_{w_{MVDR}} \min(w^H R_y w) = \min E[|y(t)|^2]$$

$$\Rightarrow \min_w P(\theta,\phi) = \{w^H R_y w\} \quad s.t. \quad w^H a(\theta_s,\phi_s) = 1 \tag{19}$$

where $P(\theta,\phi)$denotes the mean output power, the beampattern can be given as [24]:

$$beampattern = 20\log_{10}\frac{|P(\theta,\phi)|}{|P(\theta,\phi)|_{Max}} \tag{20}$$

This method reduces the contribution of the unwanted signal by minimizing the power of output noise and interference and ensuring the power of useful signal equals to 1 (constant) in the direction of useful signal $w^H a(\theta_s,\phi_s)=1$. By using Lagrange multiplier, the MVDR weight vector that gives the solution for the above equation as per the following formula [25]:

$$w_{MVDR} = \frac{a(\theta_s,\phi_s)R_y^{-1}}{a^H(\theta_s,\phi_s)R_y^{-1}a(\theta_s,\phi_s)} \tag{21}$$

Inserting Eq. (21) into Eq. (11), the output of MVDR beamformer is given by;

$$\begin{aligned} y(t) &= w^H(t)\,x_T(t) \\ &= w^H a(\theta_s)\,x_s(t) + w^H x_i(t)\,a(\theta_i) + w^H x_n(t) \\ &= x_s(t) + w^H x_i(t)\,a(\theta_i) + w^H x_n(t) \end{aligned} \tag{22}$$

The output signal power of the array as a function of the DoA estimation, using optimum weight vector from MVDR beamforming method [26], it is given by MVDR spatial spectrum for angle of arrival estimated by detecting the peaks in this angular spectrum as [7]:

$$P_{MVDR}(\theta) = \frac{1}{a^H(\theta_s,\phi_s)R_y^{-1}a(\theta_s,\phi_s)} \tag{23}$$

Finally, the SINR is defined as the ratio of the average power of the desired signal divided by the average power of the undesired signal:

$$SINR = \frac{\mathrm{E}\{|y_s(t)|^2\}}{\mathrm{E}\{|y_{i+n}(t)|^2\}} = \frac{w^H R_s w}{w^H R_{i+n} w} \tag{24}$$

3. Simulation Results and Analysis

In this study, *L*-elements linear antenna array configuration is arranged along some axis added to the beamformer system at the *BS*. The array receives signals from different spatially separated users. The received signal consists of the intended signal, co-channel interference, and a random noise component. To increase the output power of the desired signal and reduce the power of co-channel interference and noise, BF is employed at the BS. The

ABF performance analysis shows an array of even and an odd number of elements that separated by interelement spacing, d, at a carrier frequency (Fc) of 2.6 GHz. The 2.6 GHz is the spectrum band allocated to LTE operators in Malaysia [27]. To measure the performance of the MVDR algorithm for ABF applications with varying parameters like the number of array sensors, the separation between the array elements, the number of SNOIs, accuracy to distinguish interference source in the location very close to the SOI, finite length samples, and noise power.

MVDR algorithm can be used in multiple user environments, whereas the goal of this study is to place a deep null in the unwanted directions with a single desired user in the base station and hence improving the overall system capacity. The analysis of each parameter mentioned above that achieve the best beamforming capabilities to form the maximum power in the SOI direction and null in the directions of interference with highest SINR output. Four different scenarios are considered, and the simulation parameters setting in this paper are shown in Table 1.

Table 1. Key simulation parameters of MVDR beamformer.

Key system parameters	Values
Array antenna configuration	Linear antenna array (LAA)
Antenna type	Isotropic
Carrier frequency (Fc)	2.6 GHz
Beam scanning range (θ, ϕ)	(0°-180°, 0°-90°)
Number of elements (L)	5, 8, 11, 16
Element spacing (d)	λ/8, λ/4, λ/2, λ
# SNOIs	1, 2, 3, 4
Noise power label (σ_n)	-50, -10, 10, 50
Snapshots (ns)	10, 50, 250, 500

3.1. The first scenario

The first simulation scenario depicted the results calculated by considering the distance between array elements are fixed to 0.5λ. The MVDR system during DoA estimation was evaluated by changing the number of array sensors. Figure 2 illustrates the spatial spectrum of MVDR estimator for the source directions implemented in this scenario. Consider a uniform linear antenna array with L=5, 8, 11, and 16-elements plus a background noise is modeled as a complex zero-mean white Gaussian noise used to estimate K directional sources at each sensor. Three undesired sources are assumed to have AoAs (θ_i) at ±60º and 0º respectively. The SOI is considered to be a plane wave from the presumed direction θ_s = 30º. The reference element is at the one-end side of the array of an odd and an even number of elements. The obtained results provide evidence that the received signals identified the SOI and SNOIs perfectly as assumed by producing peaks in the directions of -60º, 0º, 30º and 60º azimuth angles respectively, which are computed using Eq. (23), where peak points of the spectrum are shown for clear observation. The peaks become sharper and accurate

resolution of MVDR spectrum estimator to find the source direction by adding more elements in the array.

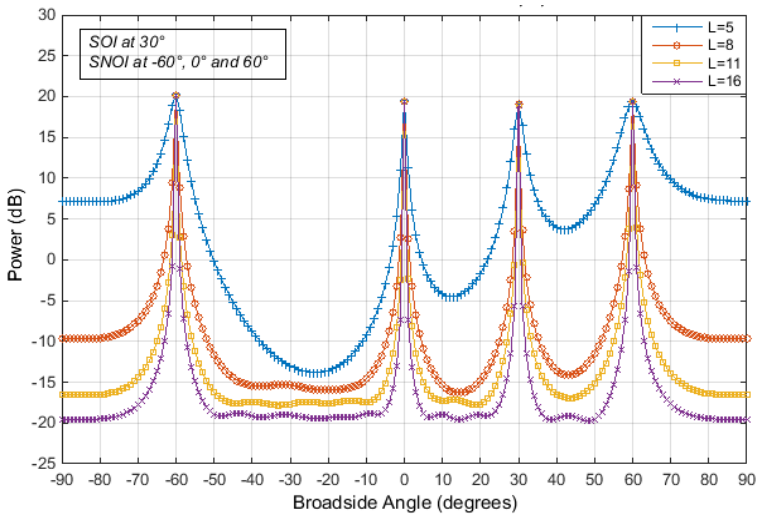

Fig. 2. MVDR-DoA estimation analysis for varying number of elements.

With the direction of the incoming signals known or estimated, the next step is to use the MVDR ABF technique to improve the signal performance of the desired target and nullifying interference directions. Figures 3 and 4 show a typical 2D beampattern plot displayed in both rectangular and polar coordinates, which demonstrate the effect if the number of elements is increased for SOI at (30º, 0º) and *SNOIs* at (±60º, 0º) and (0º, 0º) respectively. This simulation was repeated for 5, 8, 11, and 16-antenna elements with an input SNR of 10dB and data samples=300. The plots observe that the MVDR successfully introduce null at the interference source, and it provides maximum gain to the look direction of the SOI. Moreover, the result of increasing the number of elements is a narrower beamwidth which is very useful in directing the antenna beam to the desired user while the number of nulls in the pattern increases. The number of side lobes (SLs) increases, whereas the level of the first and subsequent SLs decreases compared to the mainbeam. SLs represent power radiated in potentially unwanted directions.

In a wireless communications system that is using antenna arrays, the SLs will contribute to the level of interference radiated in the cell by a transmitter as well as the level of interference seen by a receiver. Therefore, the increases in a number of elements in a linear array would result in higher directivity, as well as a sharper and narrower main lobe beamwidth. The main lobe beamwidth (MLBw), maximum side lobe level (MSLL) that is closest to the main beam, maximum depth null (MDN) at interference direction and output SINR are shown in Table 2. On the other hand, the computing operations become more complex. Besides, the implementation cost of the array increases as more sensors are used, due to the increasing number of RF modules, A/D converters.

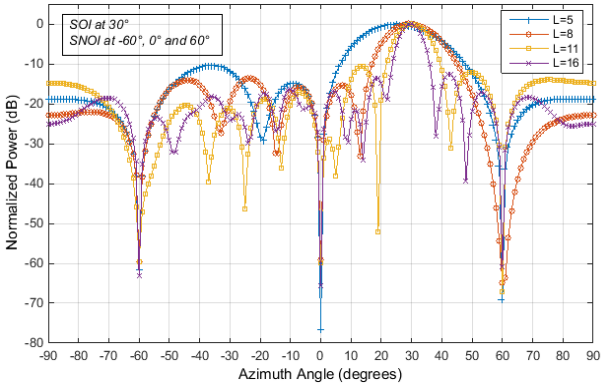

Fig. 3. Line plot - beampattern analysis of MVDR varying L=5, 8, 11, and 16 with $d=\lambda/2$.

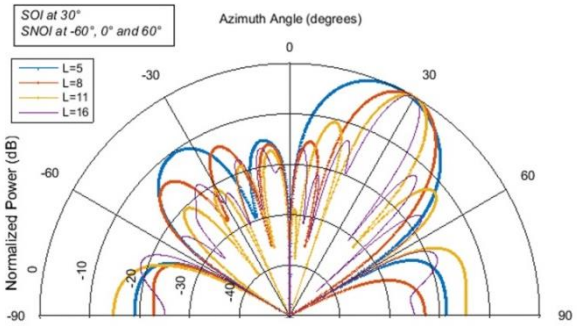

Fig. 4. Polar plot - beampattern analysis of MVDR varying L = 5, 8, 11, and 16 with $d=\lambda/2$.

Table 2. MVDR performance analysis for SOI at 30° and SNOIs at -60º, 0º and 60º with varying L.

L	d [m]	MLBw [30°]	MSLL [dB]	MDN [dB]	SINR [dB]
5	$\lambda/2$ [0.057]	60°	-14.8	-76.2	55.8
8		47°	-15.3	-64.7	56.5
11		24°	-10.6	-67.1	57.9
16		16°	-12.6	-65.6	59.4

3.2. The second scenario

One of the important parameters in the design of an antenna array is the separation space between the array elements. Second simulation scenario illustrates the results calculated by considering an 8-elements with interelement spacing of one-eighth wavelength ($\lambda/8$), a quarter wavelength ($\lambda/4$), half wavelength ($\lambda/2$), and full wavelength (λ) for SOI at 30° and SNOIs at -60°, 0°, 60°.

Figures 5 and 6 display the rectangular and polar plots that demonstrate the effect of the element spacing on MVDR performance. It is found that for $d=\lambda/8$ and $\lambda/4$, the mainlobe beamwidth is approximately the same whereas the narrowest

mainbeam is achieved when the sensors separated by λ. However, as element spacing of full wavelength the grating lobe appears on -30° azimuth with almost equal gain for the mainbeam which leads to MVDR performance degradation. The coupling effects appear when elements are spaced closely as shown in Fig. 6 for $d=\lambda/8$ at -27° with a power of -0.5dB. The SLL that is closest to the mainbeam for each interelement spacing has a height of -0.5dB, -8.8dB, -15.3dB, and -13.2dB at -27°, 90°, 7°, and 19° respectively. Furthermore, if the spacing is less than $\lambda/2$, it does not improve the MVDR performance in terms of resolution, and the coupling effects will be bigger and tend to reduce as space increases. If the spacing is greater than $\lambda/2$, this causes grating lobes that degrade the MVDR performance as well. Thus, the spacing has to be $\leq \lambda/2$ to avoid grating lobes, and the interelement separation has to be spaced enough to prevent mutual coupling. As the spacing between elements increases, the mainlobe beamwidth decreases, the number of SLs also increases and the highest output SINR obtained from $\lambda/2$ as depicted in Table 3. Besides, increasing d produces a sharper beam and the angle of the grating lobe is not a function of L, but it relies on d. It is observed that an increase in interelement spacing in an LAA will result in higher directivity and a smaller beamwidth. Although this is a favorable condition, it is found that the number of undesirable SLs also increases with increasing d.

3.3. The third scenario

Using multiple antennas at the BS can reduce the effects of co-channel interferenc e, multipath fading, and background noise. Many BF algorithms have been devise d to cancel interference sources that appear in the cellular system. MVDR algorith m can null the interferences without any distortion to the desired path.

To study the effect of SNOIs on the MVDR performance is highlighted in this part. The subsequent MVDR pattern plots with cancellation for all interferences are shown in Fig. 7. It shows the 3D power spectrum for an eight-element linear array in the presence of a different angle of arrival (AoA) for SOI and SNOIs. In Fig. 7, the output of MVDR BF algorithm is illustrated against a different number of interference sources as listed in Table 4. The elevation angle is assumed to be $\phi_s=\phi_i=0°$ for all cases. Assume a single desired user signal at 40° azimuth angle with a single interference source at 0° azimuth angle as shown in Fig. 7(a). Figure 7(b) shows the SOI direction at 0° with two SNOIs at 40° and 60°. Figure 7(c) deals with three undesired sources at -60°, 0°, and 50° directions respectively with single desired signal direction at -20°.

Four unwanted signals arrive from 0°, 15°, 45° and 60° with real user angle at 30° as illustrated in Fig. 7(d). It can be seen that the performance of the MVDR is affected by the number of SNOIs, as the number of SNOI increases, the SINR decreases with 10° null widths in the elevation angles. MVDR technique is distortionless to SOI with respect to the i^{th} signal and places a perfect null of the other L-1 signals. In the case of two interference sources, the deep null of -68.7dB compared to -48.5dB for 16-elements was found for a study conducted by [18] based on conjugate gradient method ABF algorithm. For 4 interference sources, the MVDR was capable of forming the mainlobe to reach the look angle even for the closer interference to the real user direction, which is the same result obtained by using enhanced MVDR model proposed by [8].

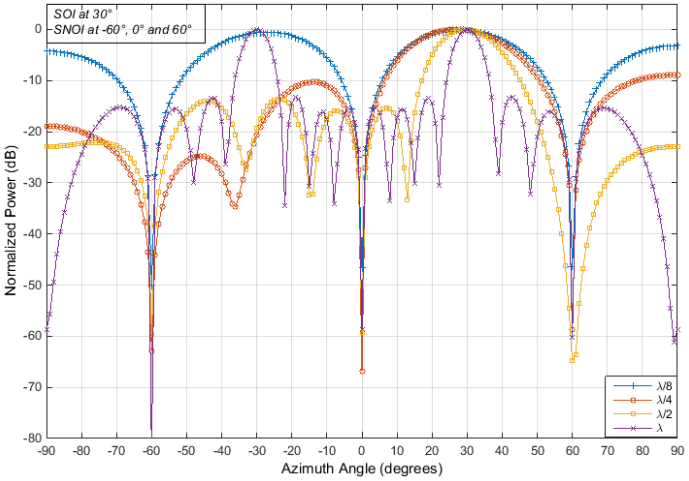

Fig. 5. Line plot - beampattern analysis of MVDR varying $d = \lambda/8, \lambda/4, \lambda/2$, and λ with L=8.

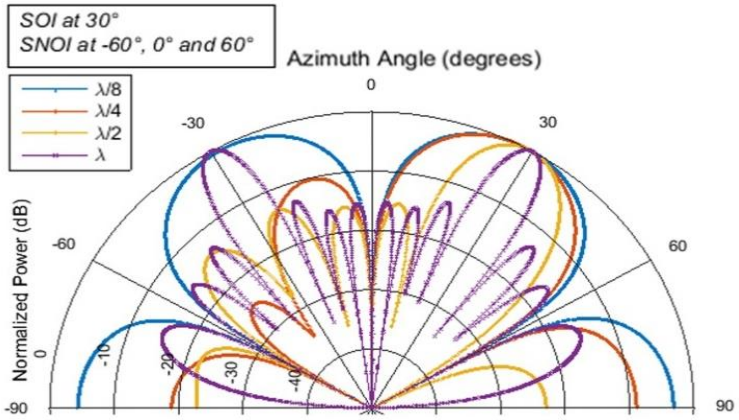

Fig. 6. Polar plot - beampattern analysis of MVDR varying $d = \lambda/8, \lambda/4, \lambda/2$, and λ with L=8.

Table 3. MVDR performance analysis for SOI at 30° and SNOIs at -60°, -30°, 0° and 60° with different *d*.

L	*d* [m]	MLBw [30°]	MSLL [dB]	MDN [dB]	SINR [dB]
8	$\lambda/8$ [0.014]	60°	-0.5	-50.0	42.5
	$\lambda/4$ [0.028]	60°	-8.8	-66.6	56.3
	$\lambda/2$ [0.057]	47°	-15.3	-64.7	56.6
	λ [0.115]	17°	-13.2	-83.2	53.8

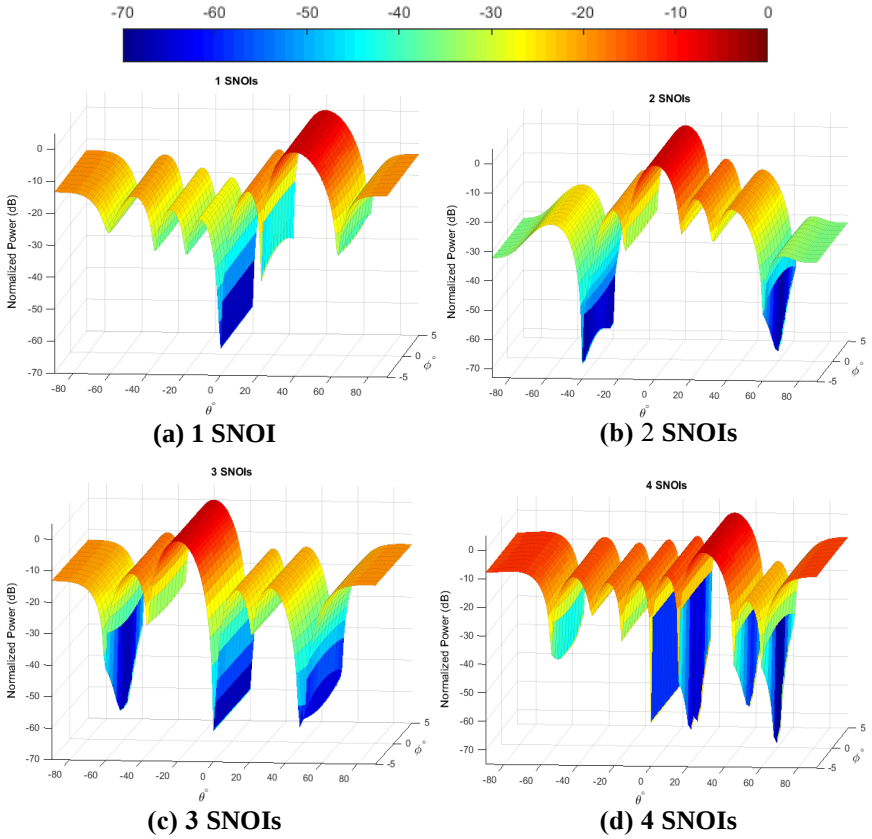

(a) 1 SNOI **(b) 2 SNOIs**

(c) 3 SNOIs **(d) 4 SNOIs**

Fig. 7. 3D beampattern analysis for MVDR for L= 8 and d=λ/2 with a different number of SNOIs and AoAs.

Table 4. Comparison of SINR values for L= 8 and d=λ/2 with a different number of SNOIs and AoAs.

L	d [m]	SOI [θ°,0°]	SNOIs [θ°,0°]	MLBw [30°]	MSLL [dB]	MDN [dB]	SINR [dB]
8	λ/2 [0.057]	40	0	40	-12.4	-62.6	63.6
		0	-40, 60	31	-11.2	-68.7	61.0
		-20	-60, 0, 50	36	-10.6	-60.2	56.6
		30	0, 15, 45, 60	30	-8.0	-73.3	54.2

3.4. The fourth scenario

In the last scenario, the effect of noise power, σ_n, and the number of snapshots, ns, on the MVDR performance are studied. The real user impinging from 30° and the unwanted sources from (±60°, 0º) and (0°, 0º) with eight sensors and the separation between sensors are λ/2. Figures 8(a)-(d) shows the output power pattern for four noise power labels ranging from -50dB to 50dB. It can be seen that the radiation pattern is approximately

similar in term of mainlobe beampattern. Figures 9(a)-(d) show the 3D power pattern of MVDR beamformer against the σ_n. The maximum null-forming obtained by using MVDR algorithm is -105dB, -64dB, -39dB and -33dB for σ_n of -50dB, -10dB, 10dB and 50dB, respectively. The corresponding SINR are 95dB, 55dB, 34dB and 21dB, respectively. Furthermore, at higher values of σ_n the MVDR still can place null to the non-look direction and the null width in the elevation angle become wider. The output SINR increases as the σ_n decreases. Besides, the reduction (negative power) at lower values of σ_n is deeper and sharper as highlighted in Fig. 9(a) than at higher values of σ_n and hence, the MVDR performance is sensitive to σ_n increases as detailed in Table 5. It is clearly shown in Fig. 9(a) for a null in the -60° azimuth with 1° elevation as compared to Fig. 9(b) for a null in the -60° azimuth with 8 elevation degree as noise power increases from -50dB to -10dB.

Additionally, in Figs. 10 and 11, the power pattern of MVDR algorithm in linear and polar shape is illustrated against the length of the data samples and evaluated by the output SINR and beampattern accuracy. As can be seen, by changing the *ns* the performance of the MVDR is affected due to the MVDR is statistical adaptive beamformer depending on the data samples. When increasing the number of *ns* is resulting in more accurate resolution also the computational time tend to increase. In term of required computational time, it is found that the required processing time for MVDR increases with the data samples increases as displayed in Table 6.

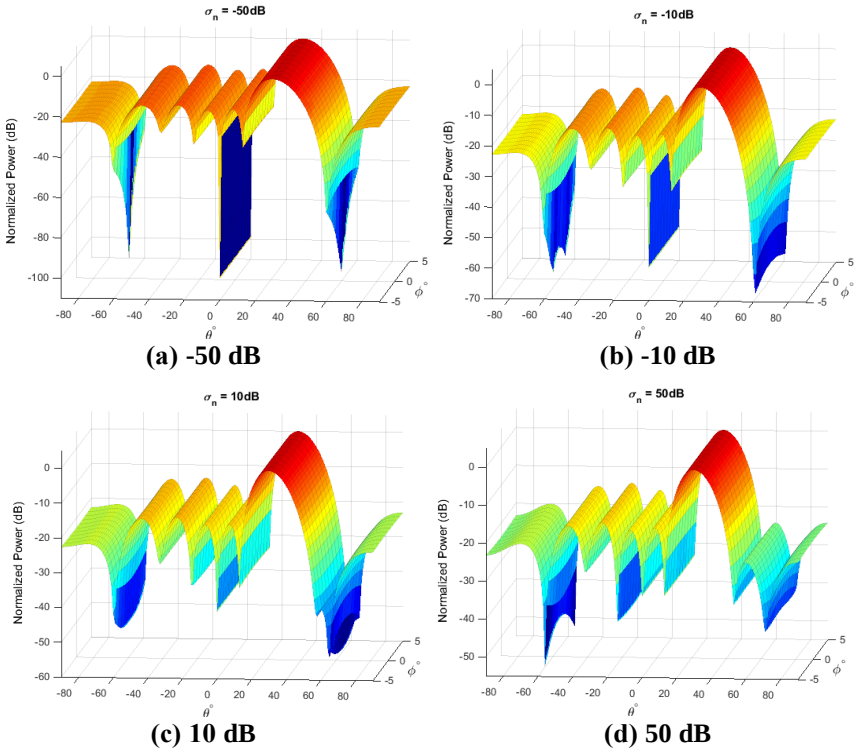

(a) -50 dB **(b) -10 dB**

(c) 10 dB **(d) 50 dB**

Fig. 8. 3D beampattern analysis for MVDR for σ_n with L=8, d=λ/2.

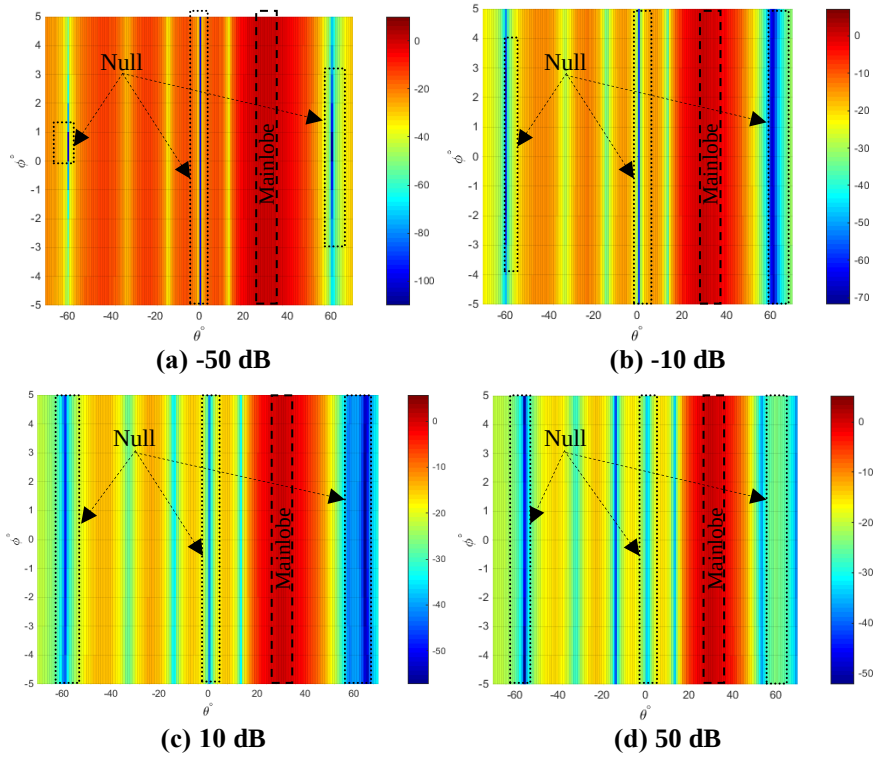

(a) -50 dB **(b) -10 dB**

(c) 10 dB **(d) 50 dB**

Fig. 9. 3D beampattern analysis for MVDR for σ_n with L=8, d=λ/2.

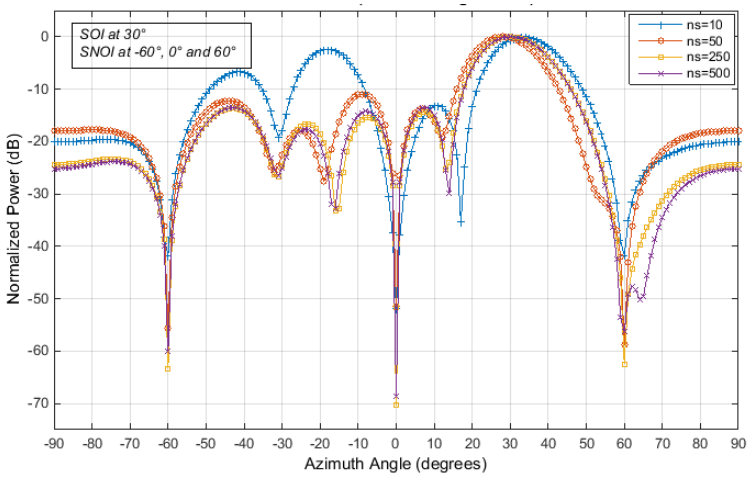

Fig. 10. Line plot - beampattern analysis of MVDR varying *ns* = 10, 50, 250, and 500 with L=8, d=λ/2.

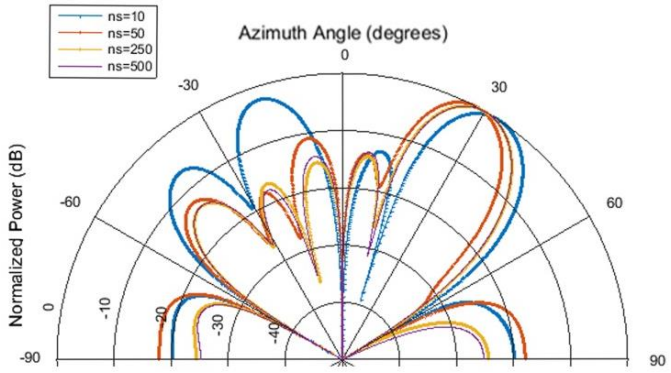

Fig. 11. Polar plot - beampattern analysis of MVDR varying *ns* = 10, 50, 250, and 500 with *L*=8, *d*=λ/2.

Table 5. MVDR performance analysis for SOI at 30° and SNOIs at -60º, -30º, 0º and 60º with different σ_n.

L	*d* [m]	σ_n [dB]	MLBw [30°]	MSLL [dB]	MDN [dB]	SINR [dB]
8	λ/2 [0.057]	-50	47°	-15.2	-105.2	95.8
		-10	46°	-15.3	-64.7	55.8
		10	44°	-15.4	-39.1	34.4
		50	43°	-15.4	-33.4	21.3

Table 6. MVDR performance analysis for SOI at 30° and SNOIs at -60º, -30º, 0º and 60º with different *ns*.

L	*d* [m]	ns	MLBw[30°]	MSLL[dB]	MDN[dB]	SINR[dB]	Time[Sec]
8	λ/2 [0.057]	10	45°	-13.0	-51.3	38.0	1.07
		50	48°	-13.8	-58.6	49.2	1.2
		250	47°	-14.3	-70.3	54.4	1.6
		500	46°	-13.5	-68.5	59.6	2.2

As seen in Table 5, the mainlobe beamwidth (MLBw) decreases and the maximum side lobe level (MSLL) slightly changes as σ_n increases while the null-forming level and SINR are strongly affected by σ_n increases. Approximately, the SINR value decreases by 1dB as the noise level increases by 1dB. In addition, Table 6 shows the SINR increases as *ns* increases owing to the increasing probability of finding a better solution. In other words, sharper and deeper nulls would be produced and hence improve the SINR by increasing *ns*. Table 7 compares the number of elements, MSLL, MDN, and SINR between the proposed approach and some of the recent studies on MVDR and other beamforming techniques. It can be noted that the MVDR based ULA give higher SINR with lower SLL with a small number of array elements. Finally, the summary of the impact of *L*, *d*, σ_n, and *ns* on the MVDR performance for a tradeoff analysis is presented in Table 8.

Table 7. A comparison between beamforming methods.

Method	*L*	*d* [m]	*ns*	MSLL [dB]	MDN [dB]	Iteration	SINR [dB]
$MVDR_{Robust}$ [19]	10	0.5λ	High	-13.8	-49.2	1	29.9
CGM [18]	8	0.5λ	Low	-8.3	-46.8	5	38.2
$MVDR_{ULA\text{-}center}$ [8]	9	0.5λ	Medium	-4.0	-50.0	1	44.4
$MVDR_{RAA}$ [20]	16	0.5λ	Medium	-12.9	-81.9	1	54.9
$MVDR_{ULA}$	8	0.5λ	Medium	-15.3	-64.7	1	56.5

Table 8. MVDR trade-off analysis.

	Pros	Cons	Performance Impact
L	- Lower SLLs - More and deeper nulls - Narrower beam - More degree of freedom - Higher SINR	- More SLLs - Larger size - More costly - Physical limitations on Installation - Complexity	- Better interference cancellation capabilities - Improved performance because of higher SINR and narrower beams
d	- Narrower beam - Lower SLLs - Higher SINR - Cost-efficient	- Grating lobes - Mutual couplin-g effects	- Grating lobes and mutual coupling have negative impact on MVDR beamformer - Wasted power in unnecessary direction
σ_n	- Higher SINR - Deeper null	- Lower SINR - Reduce null level	- Improved performance because of higher SINR
ns	- More accurate resolution - Deeper null Higher SINR	- Time consuming	- Improved performance because of s higher SINR

4. Conclusions

MVDR algorithm has gained significance in the wireless cellular communication system due to its capability to diminish co-channel and adjacent channel interference and raised SINR helps to improve system capacity. The MVDR with LAA is tested with different numbers of antenna elements, varying the separation between elements, a different number of interference sources with varying angular separations between SOI and the interference sources, different labels of noise power, and different length of data samples. Beam-steering and null-forming for MVDR beamformer is compared analytically and numerically with the rectangular geometry. It is observed that the MVDR based linear antenna structure is a suitable implementation technique for commercial wireless communication applications, due to its low complexity, low cost, higher SINR and possible integration with existing cellular base stations. The null-forming examples

nulls deeper than -64dB are recorded using 8-LAA with SINR of 56.5dB compared to SINR 54.9dB by using 16-RAA [20]. The null-forming for MVDR is sensitive as σ_n varying. MVDR can provide accurate beampattern even in the multiple signal environments. An increased number of data samples result in higher SINR and accurate beampattern. An ongoing research extends the results of this paper to enhance MVDR algorithm based on arbitra ry antenna array geometry.

Acknowledgments

This research is sponsored by the research grant number (RDU 160351) funded by University Malaysia Pahang.

References

1. Cisco Visual Networking Index (2014). Global mobile data traffic forecast update, 2013-2018, *white paper*, Cisco Systems Inc. San Jose, CA, USA.
2. Ericsson Mobility Report (2015). On the pulse of the networked society. Ericsson: Kista, Sweden.
3. Liberti, J.C.; and Rappaport T.S. (1999). *Smart antennas for wireless communications: IS-95 and third generation CDMA applications.* Prentice Hall PTR.
4. Halim, M.A. (2001). *Adaptive array measurements in communications* (1st ed.). Norwood, MA, USA: Artech House Publichers.
5. Okkonen, J. (2013). *Uniform linear adaptive antenna array beamforming implementation with a wireless open-access research platform.* Master thesis, Department of Computer Science and Engineering, University of Oulu, Finland.
6. Pan, C.; Chen J.; and Benesty J. (2014). Performance study of the MVDR beamformer as a function of the source incidence angle. *IEEE/ACM Transactions on Audio, Speech, and Language Processing*, 22(1), 67-79.
7. Khaldoon, A.O.; Rahman, M.M.; Ahmad, R.B.; and Hassnawi, L.A. (2014). Enhanced uniform linear array performance using modified minimum variance distortionless response beamformer algorithm. *Proceedings of the Second International Conference on Electronic Design (ICED).* Penang, Malaysia, 198-203.
8. Lin, J.R.; Peng, Q.C.; and Shao, H.Z. (2007). On diagonal loading for robust adaptive beamforming based on worst-case performance optimization. *ETRI journal*, 29(1), 50-58.
9. Manolakis, D.G.; Ingle, V.K.; and Kogon, S.M. (2005). *Statistical and adaptive signal processing: spectral estimation, signal modeling, adaptive filtering, and array processing.* Norwood, MA, USA: Artech House, Inc.
10. Das, K.J.; and Sarma, K.K. (2012). Adaptive beamforming for efficient interference suppression using minimum variance distortionless response. *Proceedings of the International Conference on Advancement in Engineering Studies & Technology*. Puducherry, India, 82-86.
11. Choi, R.L.U.; Murch, R.D.; and Letaief, K. (2003). MIMO CDMA antenna system for SINR enhancement. *IEEE Transactions on Wireless Communications,* 2(2), 240-249.

12. Serbetli, S.; and Yener A. (2004). Transceiver optimization for multiuser MIMO systems. *IEEE Transactions on Signal Processing*, 52(1), 214-226.
13. Kum, D.; Kang, D.; and Choi, S. (2014). Novel SINR-based user selection for an MU-MIMO system with limited feedback. *ETRI Journal*, 36(1), 62-68.
14. Rao, A.P.; and Sarma N. (2014). Performance analysis of differential evolution algorithm based beamforming for smart antenna systems. *International Journal of Wireless and Microwave Technologies*, 4(1), 1-9.
15. Ku, B. J.; Ahn, D. S.; Lee, S.P.; Shishlov, A.; Reutov, A.; Ganin, S.; and Shubov, A. (2002). Radiation pattern of multibeam array antenna with digital beamforming for stratospheric communication system: statistical simulation. *ETRI journal*, 24(3), 197-204.
16. Habets, E.; Benesty, J.; Cohen, I.; Gannot, S.; and Dmochowski, J. (2010). New insights into the MVDR beamformer in room acoustics. *IEEE Transactions on Audio, Speech, and Language Processing*, 18(1), 158-170.
17. Saxena, P.; and Kothari, A. (2014). Performance analysis of adaptive beamforming algorithms for smart antennas. *IERI Procedia*, *Elsevier*, 10, 131-137.
18. Mu, P.; Li, D.; Yin, Q.; and Guo, W. (2013). Robust MVDR beamforming based on covariance matrix reconstruction. *Science China Information Sciences*, 56, 1-12.
19. Shahab, S.N.; Zainun, A.R.; Noordin, N.H.; and Mohamad, A.J. (2015). Performance analysis of smart antenna based on MVDR beamformer using rectangular antenna array. *ARPN Journal of Engineering and Applied Sciences*, 10(22), 17132-17138.
20. Lee, M.-S. (2009). Wideband Capon beamforming for a planar phased radar array with antenna switching. *ETRI journal*, 31(3), 321-323.
21. Godara, L.C. (2004). *Smart antennas*. Boca Raton: CRC press.
22. Souden, M.; Benesty J.; and Affes, S. (2010). A study of the LCMV and MVDR noise reduction filters. *IEEE Transactions on Signal Processing*, 58(9), 4925-4935.
23. Godara, L.C. (1997). Application of antenna arrays to mobile communications. II. Beam-forming and direction-of-arrival considerations. *Proceedings of the IEEE*, 85(8), 1195-1245.
24. Renzhou, G. (2007). Suppressing radio frequency interferences with adaptive beamformer based on weight iterative algorithm. *Proceedings of the Conference on Wireless, Mobile and Sensor Networks (CCWMSN07).* Shanghai, China, 648-651.
25. Haykin, S. (2013) *Adaptive filter theory* (4th ed.). Prentice Hall.
26. Capon, J. (1969). High-resolution frequency-wavenumber spectrum analysis. *Proceedings of the IEEE*, 57(8), 1408-1418.
27. Malaysian Communications and Multimedia Commission (2011). SKMM-MCMC Annual Report.; Retrieved February 25, 2013, from: http://www.skmm.gov.my/skmmgovmy/media/General/pdf/.